

Gravitational Radiation from Primordial Helical Inverse Cascade MHD Turbulence

Tina Kahniashvili,^{1,2,3} Leonardo Campanelli,^{4,5} Grigol Gogoberidze,^{6,1,3} Yurii Maravin,¹ and Bharat Ratra¹

¹*Department of Physics, Kansas State University, 116 Cardwell Hall, Manhattan, KS 66506, USA*

²*Department of Physics, Laurentian University, Ramsey Lake Road, Sudbury, ON P3E 2C6, Canada*

³*National Astrophysical Observatory, Ilia Chavchavadze State University, 2A Kazbegi Ave, Tbilisi, GE-0160, Georgia*

⁴*Dipartimento di Fisica, Università di Bari, I-70126 Bari, Italy*

⁵*INFN - Sezione di Bari, I-70126 Bari, Italy*

⁶*Centre for Plasma Astrophysics, K.U. Leuven, Celestijnenlaan 200B, 3001 Leuven, Belgium*

(Dated: July 2, 2021)

We consider the generation of gravitational waves by primordial helical inverse cascade magneto-hydrodynamic (MHD) turbulence produced by bubble collisions at the electroweak phase transition. We extend the previous study [1] by considering both currently discussed models of MHD turbulence. For popular electroweak phase transition parameter values, the generated gravitational wave spectrum is only weakly dependent on the MHD turbulence model. Compared to the unmagnetized electroweak phase transition case, the spectrum of MHD-turbulence-generated gravitational waves peaks at lower frequency with larger amplitude and can be detected by the proposed Laser Interferometer Space Antenna.

PACS numbers: 98.70.Vc, 98.80.-k

I. INTRODUCTION

The direct detection of a gravitational wave background will provide us with a probe of physical conditions in the early Universe at the epoch when the gravitational radiation was generated. This is because gravitational waves are massless and after generation weakly-coupled gravitational radiation propagates freely. Hence, once generated, any gravitational wave spectrum retains its shape, with all wavelengths simply scaling with the expansion of the Universe. Gravitational wave astronomy holds the potential for helping construct a picture of the Universe at energy scales even higher than those the Large Hadron Collider will reach, to probe in detail physics at the electroweak energy scale.

There are various mechanisms that might generate gravitational waves in the early Universe, for reviews see [2, 3]. A well-known one is parametric amplification of quantum fluctuations [4], which can also take place shortly after inflation [5]. Other mechanisms include bubble wall motion and collisions during phase transitions; gravitational wave generation during the electroweak and QCD phase transitions are discussed in Refs. [6, 7, 8, 9, 10]. Cosmic strings and other defects can produce relic gravitational waves [11]. Cosmological magnetic fields [12, 13, 14] and hydrodynamical or magnetohydrodynamical turbulence can also induce primordial gravitational waves [1, 15, 16, 17, 18].

Gravitational waves will also provide information on symmetries present in the Universe. In particular, the relic gravitational wave background carries information about parity asymmetry, that might be generated at the electroweak phase transition, or earlier. Parity symmetry testing based on the direct detection of gravitational waves in the near future (with currently planned missions) seems to be promising for gravitational waves with frequencies around the Laser Interferometer Space Antenna (LISA) sensitivity band at 0.1 – 100 mHz [19]. The Standard Model electroweak phase transition, when parity symmetry breaking and magnetic helicity production might be expected [20], produces gravitational waves with a significant amplitude in this frequency range. Recently, some of us have investigated the generation of gravitational waves through inverse cascade MHD turbulence [1] and found that even a small amount of initial helicity enlarges the range of phase transition parameters for which gravitational waves are potentially detectable by LISA. This gravitational wave signal has an important feature: it is circularly polarized. For direct cascade hydrodynamical turbulence some of us have previously estimated the polarization degree [17], which is obviously turbulence model dependent. Polarized gravitational waves are present in other models [21], and the polarization of the gravitational wave background is in principle observable, either directly [22] or through the cosmic microwave background [13, 23].

The detection prospects of gravitational radiation from the early Universe depend on the energy scale when gravitational waves were generated and even more so on the source duration time and efficiency of the generation process itself. In particular, to produce a detectable signal the electroweak phase transition must be strong enough [24, 25, 26]. The currently popular standard model of particle physics does not have a strong enough electroweak phase transition. Also, all currently discussed electroweak phase transition models do not predict an observable gravitational radiation signal if one assumes only bubble collisions [26]. It is of particular interest to study gravitational wave production during phase transitions in the minimal and next to minimal supersymmetric standard models (MSSM and nMSSM [27]), [8]. The gravitational wave signal produced in the MSSM model is below the LISA sensitivity, while the nMSSM results in a stronger electroweak phase transition [27] and as a consequence a detectable gravitational wave signal [8].

On the other hand, sources associated with stochastic vector fields in plasma, i.e. kinetic velocity or magnetic fields, significantly change gravitational wave detection prospects [28]. In the case of unmagnetized hydrodynamical turbulence the peak frequency of the gravitational wave power spectrum is determined by the characteristic time of turbulence, i.e. the inverse turn-over time of the largest eddy. Another important characteristic is the energy scale when gravitational radiation is generated. In recent modifications of the standard electroweak phase transition model where the transition is moved to a higher energy scale [25, 29], the gravitational wave power spectrum peak frequency is shifted to a higher frequency, which, since the gravitational wave spectrum is sharply peaked, reduces the possibility of detection by LISA. The presence of a cosmological magnetic field affects the dynamics of turbulence. In the case of MHD turbulence the presence of an energy inverse-cascade leads to an increase in the effective size of the largest eddy (now associated with a helical magnetic field), and can result in the gravitational wave power spectrum peaking in the LISA band, with amplitude large enough to be detected by LISA [1].

In this paper we extend the study of Ref. [1] by also considering a different model of MHD turbulence. In particular, Ref. [1] adopts the inverse cascade model of Refs. [30, 31], and in this paper we also include in the consideration the model of Refs. [32, 33, 34]. In both cases, gravitational wave generation is considered assuming non-zero magnetic helicity during the phase transition.

For our analysis in this paper we adapt the technique developed in Ref. [18]. We model MHD turbulence and obtain the gravitational wave spectrum by using an analogy with the theory of sound wave production by hydrodynamical turbulence [35, 36, 37, 38]. We perform the computation of the gravitational wave spectrum in real space, instead of using conventional Fourier space techniques as in Refs. [9, 15]. This makes the physical interpretation of all quantities straightforward. We use natural units with $\hbar = c = k_B = 1$ throughout.

The paper is organized as follows. In Sec. II we summarize the general formalism of gravitational wave generation. In Sec. III we describe the turbulence models we consider. In Sec. IV we derive the gravitational wave spectra, and we conclude in Sec. V.

II. GRAVITATIONAL WAVE GENERATION FORMALISM

We assume that primordial turbulence is generated at time t_* — corresponding to temperature T_* at the phase transition — at characteristic proper length-scale $l_0 = 2\pi/k_0$ (where k_0 is the corresponding proper wavenumber) and with characteristic velocity perturbation v_0 . We assume that the kinetic and magnetic Reynolds numbers are much greater than unity on scales of order l_0 , otherwise there is no turbulence. We also assume that the duration of the turbulence, τ_T , is no larger than the Hubble time at the phase transition H_*^{-1} , where H_* is the value of the Hubble parameter at the phase transition, so the expansion of the Universe may be neglected during the generation of gravitational radiation [15, 16]. This adiabatic assumption will be valid for any turbulence produced in a realistic cosmological phase transition [39]. Therefore, the gravitational radiation equation in real space can be written as [40]

$$\nabla^2 h_{ij}(\mathbf{x}, t) - \frac{\partial^2}{\partial t^2} h_{ij}(\mathbf{x}, t) = -16\pi G S_{ij}(\mathbf{x}, t), \quad (1)$$

where $h_{ij}(\mathbf{x}, t)$ is the tensor metric perturbation, t is physical time, i and j are spatial indices (repeated indices are summed), and G is the gravitational constant. S_{ij} is the traceless part of the stress-energy tensor $T_{ij}(\mathbf{x}, t)$, (constructed from either kinetic or magnetic turbulence vector fields), given by [40]

$$S_{ij}(\mathbf{x}, t) = T_{ij}(\mathbf{x}, t) - \frac{1}{3} \delta_{ij} T_k^k(\mathbf{x}, t). \quad (2)$$

Since the turbulent fluctuations are stochastic, so are the generated gravitational waves. Our goal is to derive the energy density spectrum of these gravitational wave perturbations at the end of the turbulent phase; after that the amplitude and wavelength of the gravitational radiation scales simply with the expansion of the Universe. The energy density of gravitational waves is [3]

$$\rho_{GW}(\mathbf{x}, t) = \frac{1}{32\pi G} \langle \partial_t h_{ij}(\mathbf{x}, t) \partial_t h_{ij}(\mathbf{x}, t) \rangle = \frac{G}{2\pi} \int d^3\mathbf{x}' d^3\mathbf{x}'' \frac{\langle \partial_t S_{ij}(\mathbf{x}', t') \partial_t S_{ij}(\mathbf{x}'', t'') \rangle}{|\mathbf{x} - \mathbf{x}'| |\mathbf{x} - \mathbf{x}''|}, \quad (3)$$

where the brackets denote an ensemble average over realization of the stochastic source, and the times $t' = t - |\mathbf{x} - \mathbf{x}'|$, $t'' = t - |\mathbf{x} - \mathbf{x}''|$.

We consider metric perturbations in the far-field limit (i.e. for $x \gg d$, where d is a characteristic length scale of the source region), where gravitational waves are the only metric perturbations [40], and replace $|\mathbf{x} - \mathbf{x}'|$ by $|\mathbf{x}|$ in Eq. (3). For the stationary turbulence we consider here, we define the gravitational wave spectral energy density,

$I(\mathbf{x}, \omega)$, as the one-dimensional temporal Fourier transform of the autocorrelation function of the temporal derivative of the tensor metric perturbations $L(\mathbf{x}, \tau)$,

$$I(\mathbf{x}, \omega) = \frac{1}{2\pi} \int d\tau e^{i\omega\tau} L(\mathbf{x}, \tau), \quad (4)$$

where ω is the angular frequency and

$$L(\mathbf{x}, \tau) = \frac{1}{32\pi G} \langle \partial_t h_{ij}(\mathbf{x}, t) \partial_t h_{ij}(\mathbf{x}, t + \tau) \rangle. \quad (5)$$

Accounting for Eq. (3), the gravitational wave energy density is

$$\rho_{\text{GW}}(\mathbf{x}) = \int d\omega I(\mathbf{x}, \omega). \quad (6)$$

Following Ref. [18] it can be shown that

$$I(\mathbf{x}, \omega) = \frac{4\pi^2 \omega^2 G w^2}{|\mathbf{x}|^2} \int d^3 \mathbf{x}' H_{ijij} \left(\mathbf{x}', \frac{\mathbf{x}}{|\mathbf{x}|} \omega, \omega \right), \quad (7)$$

where \mathbf{k} is a proper wavevector and $w = \rho + p$, with w , ρ , and p being respectively the enthalpy, pressure, and energy density of the plasma. The quantity $H_{ijij}(\mathbf{x}', \mathbf{k}, \omega)$ is the double trace of the four-dimensional temporal and spatial Fourier transform¹, taken with respect to $\mathbf{x}'' - \mathbf{x}'$ and τ , of the two-point time-delayed fourth-order correlation tensor

$$R_{ijkl}(\mathbf{x}', \boldsymbol{\xi}, \tau) = \frac{1}{w^2} \langle S_{ij}(\mathbf{x}', t) S_{kl}(\mathbf{x}'', t + \tau) \rangle. \quad (8)$$

That is,

$$H_{ijkl}(\mathbf{x}', \mathbf{k}, \omega) = \frac{1}{(2\pi)^4} \int d^3 \boldsymbol{\xi} d\tau e^{i(\omega\tau - \mathbf{k} \cdot \boldsymbol{\xi})} R_{ijkl}(\mathbf{x}', \boldsymbol{\xi}, \tau), \quad (9)$$

where $\boldsymbol{\xi} = \mathbf{x}'' - \mathbf{x}'$.

Given the function $H_{ijkl}(\mathbf{x}', \mathbf{k}, \omega)$, we may use Eqs. (6) and (7) to compute the gravitational wave energy density, assuming that the source is statistically homogeneous, so that the averaged correlators of the stress-energy tensor have no spatial dependence, and isotropic, so that the correlation between two spatial points depends only on the distance between the points and not on the direction. With these assumptions, Eq. (9) reduces to

$$H_{ijkl}(\mathbf{x}', \mathbf{k}, \omega) = H_{ijkl}(\mathbf{k}, \omega) = \frac{1}{(2\pi)^4} \int d^3 \boldsymbol{\xi} d\tau e^{i(\omega\tau - \mathbf{k} \cdot \boldsymbol{\xi})} R_{ijkl}(\boldsymbol{\xi}, \tau), \quad (10)$$

so $H_{ijkl}(\hat{\mathbf{x}}\omega, \omega) = H_{ijkl}(\omega, \omega)$ is independent of the observation direction $\hat{\mathbf{x}}$, as expected on physical grounds.

Finally, since the gravitational waves propagate freely after been generated, the expansion of the Universe is accounted for by a simple re-scaling of the frequency and the amplitude by a factor equal to

$$\frac{a_\star}{a_0} \simeq 8 \times 10^{-16} \left(\frac{100 \text{ GeV}}{T_\star} \right) \left(\frac{100}{g_\star} \right)^{1/3}, \quad (11)$$

where g_\star is the number of relativistic degrees of freedom at the temperature T_\star . For the standard model degrees of freedom we have $g_\star = 106.75$ as $T \rightarrow \infty$. With these assumptions and considering a stochastic turbulence source lasting for a finite duration τ_T , the total gravitational radiation energy density spectrum at a spatial point and a time can be obtained by integrating over all sources within a spherical shell centered at that observer, with a shell thickness corresponding to the duration of the phase transition, and a radius equal to the proper distance along any light-like path from the observer to the source. Then we get [1, 18]

$$\rho_{\text{GW}}(\omega) = \frac{d\rho_{\text{GW}}}{d\ln \omega} = 16\pi^3 \omega^3 G w^2 \tau_T H_{ijij}(\omega, \omega), \quad (12)$$

¹ Consistent with current observational indications [41], we assume flat spatial hypersurfaces and use spatial Fourier transform relations $F_j(\mathbf{k}) = \int d^3 x e^{i\mathbf{k} \cdot \mathbf{x}} F_j(\mathbf{x})$ and $F_j(\mathbf{x}) = \int d^3 k e^{-i\mathbf{k} \cdot \mathbf{x}} F_j(\mathbf{k}) / (2\pi)^3$.

where ω is the angular frequency measured at the moment of generation of the gravitational radiation. As shown in Ref. [18], while $H_{ijij}(\omega, \omega)$ is a complicated function of ω , the resulting gravitational wave signal strength can be simply estimated with $\pm 25\%$ accuracy by working in the $\mathbf{k} \rightarrow 0$ limit and replacing $H_{ijij}(\mathbf{k}, \omega)$ by the corresponding $H_{ijij}(0, \omega)$ — this is the main point of the aero-acoustic approximation initially used for sound wave generation by turbulence [36]. It can be shown that this approximation works rather well for low velocity turbulence, with Mach number M less than unity, i.e. for $M = v_0 < 1$, where v_0 corresponds to the turbulence velocity of the largest eddy.

We assume that turbulence is caused by bubble collisions during the phase transition. In general, phase transitions can be described by two key parameters: $\alpha = \rho_{\text{vac}}/\rho_{\text{thermal}}$, the ratio of the vacuum energy density associated with the phase transition to the thermal energy density of the Universe at the time (this characterizes the strength of the phase transition); and β^{-1} , which sets the characteristic time scale for the phase transition, as well as the temperature T_* when the phase transition occurs. All other parameters, such as the efficiency factor κ which gives the fraction of the available vacuum energy which goes into the kinetic energy of the expanding bubble walls (as opposed to thermal energy), the bubble wall velocity v_b , and the turbulent eddy velocity v_0 , can be expressed through T_* , α , and β^{-1} . In particular [7, 10, 42]

$$\kappa(\alpha) = \frac{1}{1 + 0.715\alpha} \left[0.715\alpha + \frac{4}{27} \left(\frac{3\alpha}{2} \right)^{1/2} \right], \quad (13)$$

$$v_b(\alpha) = \frac{1/\sqrt{3} + (\alpha^2 + 2\alpha/3)^{1/2}}{1 + \alpha}, \quad (14)$$

$$v_0(\alpha) = \left(\frac{3\kappa\alpha}{4 + 3\kappa\alpha} \right)^{1/2}. \quad (15)$$

The parameter β^{-1} is determined from the bubble nucleation rate per unit volume $\Gamma = \Gamma_0 e^{\beta t}$ [7] where Γ_0 is determined by initial conditions. For the standard model $\beta^{-1} = 100H_*$. The temperature T_* and the Hubble parameter at the phase transition H_* are related through

$$H_*^2 = \frac{8\pi^3 G T_*^4}{90}. \quad (16)$$

In the next section we discuss two specific models for the turbulent motions.

III. TURBULENCE MODELS

In this paper we are interested in the generation of gravitational waves by helical MHD turbulence, that is turbulence in a magnetized plasma with non-vanishing magnetic helicity, \mathcal{H}_M , defined by

$$\mathcal{H}_M(t) = \int d^3x \mathbf{A} \cdot \mathbf{B}, \quad (17)$$

where \mathbf{A} is the vector potential of the magnetic field \mathbf{B} . Magnetic helicity is odd under discrete P and CP transformations, so the presence of magnetic helicity in our Universe would be an indication of macroscopic P and CP violation.

While MHD turbulence is isotropic on large scales, it is locally anisotropic on small scales [43], resulting in small-scale anisotropy in the generated GW background. However, GWs are generated mainly by the largest eddies [18] so we adopt an isotropic turbulence model with velocity field and magnetic field two-point correlation functions [35]

$$\langle v_i^*(\mathbf{k}, t) v_j(\mathbf{k}', t + \tau) \rangle = \delta(\mathbf{k} - \mathbf{k}') F_{ij}^v(\mathbf{k}, t) f[\eta(k), \tau], \quad (18)$$

$$\langle b_i^*(\mathbf{k}, t) b_j(\mathbf{k}', t + \tau) \rangle = \delta(\mathbf{k} - \mathbf{k}') F_{ij}^M(\mathbf{k}, t) f[\eta(k), \tau]. \quad (19)$$

Here \mathbf{v} is the turbulent-motion velocity field, $\mathbf{b} = \mathbf{B}/\sqrt{4\pi w}$ is the characteristic magnetic field perturbation \mathbf{B} expressed in velocity units, and

$$F_{ij}^v(\mathbf{k}, \tau) = P_{ij}(\mathbf{k}) \frac{E_v(k, t)}{4\pi k^2}, \quad (20)$$

$$F_{ij}^M(\mathbf{k}, \tau) = P_{ij}(\mathbf{k}) \frac{E_M(k, t)}{4\pi k^2} + i\epsilon_{ijl} k_l \frac{H_M(k, t)}{8\pi k^2}. \quad (21)$$

In the above equations the projection operator $P_{ij}(\mathbf{k}) = \delta_{ij} - k_i k_j / k^2$, δ_{ij} is the Kronecker delta, $k = |\mathbf{k}|$, ε_{ijkl} is the totally antisymmetric tensor, and $\eta(k)$ is an autocorrelation function that determines the characteristic function $f[\eta(k), \tau]$ describing the temporal decorrelation of turbulent fluctuations. In the following we use $f[\eta(k), \tau] = \exp[-\pi\eta^2(k)\tau^2/4]$ [44]. The function $E_v(k, t)$ in Eq. (20) is the so-called kinetic power spectrum and is related to the kinetic energy of turbulence through

$$\mathcal{E}_v(t) = \int dk E_v(k, t), \quad (22)$$

while in Eq. (21) $E_M(k, t)$ and $H_M(k, t)$, the magnetic field energy and magnetic helicity power spectra, denote the symmetric and antisymmetric parts of the two-point magnetic field correlator. They are related to the magnetic energy and magnetic helicity densities through

$$\mathcal{E}_M(t) = \int dk E_M(k, t) \quad (23)$$

and

$$\mathcal{H}_M(t) = \int dk H_M(k, t), \quad (24)$$

respectively.

It is worth noting that for all magnetic field configurations, the magnetic helicity spectrum must satisfy the “realizability condition” [45]: $|H_M(k, t)| \leq 2E_M(k, t)/k$. Introducing the magnetic correlation length (i.e., the characteristic proper length associated with the large magnetic energy eddies of turbulence),

$$\xi_M(t) = \frac{\int dk k^{-1} E_M(k, t)}{\mathcal{E}_M(t)}, \quad (25)$$

the integral form of the realizability condition is $|\mathcal{H}_M(t)| \leq 2\xi_M(t)\mathcal{E}_M(t)$. In the following, we assume that a magnetic field with (positive) magnetic helicity has been generated during a phase transition through some mechanism [20]. We also assume “small” initial magnetic helicity, in the sense that the parameter

$$\zeta_\star = \frac{\mathcal{H}_M(t_\star)}{2\xi_M(t_\star)\mathcal{E}_M(t_\star)} \quad (26)$$

is much smaller than unity.

After generation, primordial helical turbulence decays freely. While it is widely accepted in the literature that the free decay of helical MHD turbulence is a two-stage process, the details of the two stages are still under discussion. Roughly speaking, in the first stage, the system proceeds through selective decay of magnetic modes: magnetic power on small scales is washed out by turbulence effects more effectively than on large scales. During this process the magnetic correlation length grows while the magnetic energy decays in time. The first stage ends when quasi-conservation of magnetic helicity starts to trigger an inverse cascade of the magnetic field: small-scale modes are no longer completely dissipated by turbulence, rather part of their energy is now transferred to larger scales. This causes a faster growth of the correlation length and a slower dissipation of the magnetic energy in comparison to the non-helical case.

Different analyses in the literature seem to agree on the details of the first stage of direct cascade. The details of the inverse-cascade regime, however, are still being debated and there are two main models, that of Refs. [30, 31], here referred to as Model A, and that of Refs. [33, 34], which we will call Model B. In the following, we consider both models.

A. First stage: direct cascade

In both models the dynamics of the first decay stage is governed by a direct cascade of magnetic energy density lasting for a time $\tau_{s0} = s_0\tau_0$, a few times ($s_0 \sim 3 - 5$) longer than the characteristic largest-eddy turn-over time $\tau_0 = l_0/v_0 = 2\pi/k_0 v_0$.² At the end of this stage equipartition between kinetic and magnetic energies is reached [45].

² To be more precise, from the results of Refs. [33, 34], the time when the system enters the inverse-cascade regime (in Model B) could depend on the fraction of the maximal initial magnetic helicity ζ_\star . However, those results were obtained assuming an initial magnetic

During the first stage magnetic energy density flows from large to small scales and finally dissipates on the scale $l_d = 2\pi/k_d$ ($k_d \gg k_0$) where one of the Reynolds numbers becomes of order unity. Due to the selective decay effect [45] magnetic helicity is nearly conserved during this stage [31, 33]. To compute the gravitational waves generated by decaying MHD turbulence, we assume that decaying turbulence lasting for time τ_{s0} is equivalent to stationary turbulence lasting for time $\tau_{s0}/2$. This can be justified using the Proudman argument for (unmagnetized) hydrodynamical turbulence [35, 38]. Consequently, when computing the induced gravitational waves we ignore the time dependence of $E_M(k, t)$ and $H_M(k, t)$. Also, for $E_M(k, t)$ and $\eta(k)$ we use the Kolmogorov model [46] with

$$E_M(k, t) = C_K \varepsilon^{2/3} k^{-5/3}, \quad (27)$$

and

$$\eta(k) = \frac{\varepsilon^{1/3}}{\sqrt{2\pi}} k^{2/3}, \quad (28)$$

both functions being defined over the range of wavenumbers $k_0 < k < k_d$. Here C_K is a constant of order unity and $\varepsilon \simeq k_0 v_0^3$ is the energy dissipation rate per unit enthalpy. Taking into account that equipartition between kinetic and magnetic energy densities is established and maintained during Kolmogorov turbulence, the total (kinetic plus magnetic) energy density of turbulence is simply double the expression in Eq. (27).

We note that while turbulence in the early Universe has to be relativistic, we have assumed a Kolmogorov spectrum for both \mathbf{b} and \mathbf{v} , which is valid for non-relativistic turbulence. Based on arguments of Ref. [15], however, we expect that our estimate gives the correct qualitative features of the resulting gravitational radiation spectrum.

B. Second stage: inverse cascade

1. Model A

Model A has been discussed in Ref. [1]. Here, we summarize those results. At the end of the first stage turbulence relaxes to a maximally helical state [31, 33]. Accounting for conservation of magnetic helicity, the characteristic velocity and magnetic field perturbations at this stage are $v_1 \simeq \zeta_\star^{1/2} v_0$ and $b_1 \simeq \zeta_\star^{1/2} b_0$. The dynamics of the second stage is governed by a magnetic helicity inverse cascade. If both Reynolds numbers are large at the end of the first stage, magnetic helicity is conserved during the second stage. The magnetic eddy correlation length evolves as [30, 31]

$$\xi_M(t) \simeq l_0 \left(1 + \frac{t}{\tau_1}\right)^{1/2}, \quad (29)$$

where $\tau_1 \simeq l_0/v_1 = \tau_0/\zeta_\star^{1/2}$ is the characteristic eddy turn-over time at the beginning of the second stage. The magnetic and kinetic energy densities evolve as [30, 31]

$$\begin{aligned} \mathcal{E}_M(t) &\simeq w b_1^2 \left(1 + \frac{t}{\tau_1}\right)^{-1/2}, \\ \mathcal{E}_v(t) &\simeq w v_1^2 \left(1 + \frac{t}{\tau_1}\right)^{-1}. \end{aligned} \quad (30)$$

These imply that the characteristic turn-over (τ_{to}) and cascade (τ_{cas}) timescales evolve as

$$\tau_{to} \simeq \tau_{cas} \simeq \tau_1 \left(1 + \frac{t}{\tau_1}\right). \quad (31)$$

To compute the gravitational waves emitted during the second stage we use the stationary turbulence model that has the same gravitational wave output. Introducing the characteristic proper wavenumber $k_\xi(t) = 2\pi/\xi_M(t)$ and

spectrum of the form $E_M(k, 0) \propto k^p$ with p a positive real number, while in our case the initial spectrum is a red spectrum of the Kolmogorov type. In the absence of firm results on this matter, and in order to avoid inessential complications, here we assume that in both models of turbulence $\tau_{s0} = s_0 \tau_0$ with $s_0 \sim \text{few}$.

using Eq. (30) we find $\mathcal{E}_M \simeq wv_1^2 k_\xi(t)/k_0$ since $b_1 \simeq v_1$. Since the kinetic energy density is dissipated more efficiently than the magnetic one, we can neglect its contribution in the following discussion. The time when turbulence is present on scale $\xi_M(t)$ is determined by Eq. (31), which can be rewritten as

$$\tau_{\text{cas}} \simeq \tau_1 \left[\frac{k_0}{k_\xi(t)} \right]^2. \quad (32)$$

So instead of considering decaying turbulence, we consider stationary turbulence with a scale-dependent duration time (time during which the magnetic energy is present on that scale), $\tau_{s1} \simeq \tau_1 [k_0/k]^2$ (for $k = k_\xi$ this coincides with τ_{cas}).

The expression for \mathcal{E}_M yields the time-independent magnetic field energy and magnetic helicity power spectra

$$E_M(k, t) = \frac{C_1 v_1^2}{k_0} = \frac{1}{2} k H_M(k, t), \quad k_S < k < k_0. \quad (33)$$

Here C_1 is a constant of order unity, k_S is the smallest wavenumber where the inverse cascade stops, and the second equation follows from saturating the causality condition. For the second stage autocorrelation function, which is inversely proportional to the turn-over time (31), we assume

$$\eta(k) = \frac{\sqrt{2\pi}}{\tau_1} \left(\frac{k}{k_0} \right)^2, \quad (34)$$

to be as close as possible to the first stage description where $\eta(k_0) = \sqrt{2\pi}/\tau_0$.

At the largest scales there is no efficient dissipation mechanism, so the inverse cascade will be stopped at the scale $l_S(t) = 2\pi/k_S$ where either the cascade timescale τ_{cas} reaches the expansion timescale $H_\star^{-1} = H^{-1}(t_\star)$, or when the characteristic length scale $\xi_M(t) \simeq l_S$ reaches the Hubble radius. These conditions are $\zeta_\star^{-1/2} l_S^2 / v_0 l_0 \leq H_\star^{-1}$ or $l_S \leq H_\star^{-1}$ (the cascade time is scale dependent and maximal at $k = k_S$). Defining $\gamma = l_0 / H_\star^{-1} \simeq v_b H_\star \beta^{-1}$,³ it is easy to see (taking into account that v_0 , γ , and ζ_\star are less than unity) that the first condition is fulfilled first and consequently

$$\frac{k_0}{k_S} \leq \left(\frac{v_0}{\gamma} \right)^{1/2} \zeta_\star^{1/4}. \quad (35)$$

To have an inverse cascade requires $k_0/k_S \geq 1$, leading to a constraint on initial helicity: $\gamma \leq M \zeta_\star^{1/2}$.

2. Model B

Instead of assuming the MHD turbulence model of Refs. [30, 31], in this subsection we consider the alternative MHD turbulence model of Refs. [33, 34] (also see Ref. [32]) with different evolution laws for the magnetic correlation length and magnetic and kinetic energy densities,

$$\xi_M(t) \simeq l_0 \left(1 + \frac{t}{\tau_1} \right)^{2/3}, \quad (36)$$

$$\mathcal{E}_M(t) \simeq w b_1^2 \left(1 + \frac{t}{\tau_1} \right)^{-2/3}, \quad (37)$$

$$\mathcal{E}_v(t) \simeq w v_1^2 \left(1 + \frac{t}{\tau_1} \right)^{-2/3}, \quad (38)$$

respectively. Taking into account the above equations, it is easy to verify, however, that the characteristic turnover and cascade timescales evolve as in Model A.

³ Taking into account that the turbulent eddies are formed through bubble expansion and bubble collisions, the energy-containing scale l_0 is determined by the bubble wall velocity v_b and the expansion time β^{-1} as $l_0 \simeq v_b \beta^{-1}$. We note that γ determines the number ($N_{\text{eddy}} \simeq \gamma^{-3}$) of turbulent eddies within the Hubble radius H_\star^{-1} .

It should be noted that, although the magnetic and kinetic energies scale in time in the same way, equipartition is not generally reached [33]. However, if the initial ratio of kinetic and magnetic energies is taken to be of order unity, equipartition is established and lasts for all time. Applying these results to the case at hand, after the first stage of direct cascade, at the end of which equipartition between magnetic and kinetic energy is established, these follows a stage of inverse cascade which preserves equipartition of energy. Hence we conclude that kinetic energy cannot be neglected in the second stage for this particular model of turbulence. In fact the amount of gravitational radiation produced in the second stage (which, as we will see, is much greater than that generated in the first stage) is exactly twice that produced considering only magnetic energy.

Proceeding as for the discussion for Model A between Eqs. (31) and (33), we find that the relation $\mathcal{E}_M \simeq wv_1^2 [k_\xi(t)/k_0]$ does not change, whereas for the cascade timescale we get

$$\tau_{\text{cas}} \simeq \tau_1 \left[\frac{k_0}{k_\xi(t)} \right]^{3/2}. \quad (39)$$

The expression for the time-independent magnetic field energy spectrum does not change, however, now it is valid for $k_S < k < k_0$ with k_S depending on the particular model of turbulence adopted (see below).

In Model B, the autocorrelation function is

$$\eta(k) = \frac{\sqrt{2\pi}}{\tau_1} \left(\frac{k}{k_0} \right)^{3/2}, \quad (40)$$

while the conditions that determine when the inverse cascade stops are $\zeta_\star^{-1/2} l_S^{3/2} / v_0 l_0^{1/2} \leq H_\star^{-1}$ or $l_S \leq H_\star^{-1}$. However in this case it is easy to see that the former condition is fulfilled before the latter one, and, consequently, we get

$$\frac{k_0}{k_S} \leq \left(\frac{v_0}{\gamma} \right)^{2/3} \zeta_\star^{1/3}. \quad (41)$$

The condition to have an inverse cascade, $k_0/k_S \geq 1$, leads to the same constraint on initial helicity found in Model A, i.e. $\gamma \leq M\zeta_\star^{1/2}$.

C. Stress-energy tensor and source for gravitational waves

The magnetic field perturbation stress-energy tensor is

$$T_{ij}^M(\mathbf{x}, t) = w b_i(\mathbf{x}, t) b_j(\mathbf{x}, t). \quad (42)$$

For the first decay stage we compute for this magnetic part and then double the result to account for approximate magnetic and kinetic energy equipartition for Alfvén waves.

To compute the function $H_{ijij}(\mathbf{k}, \omega)$, we assume Millionshchikov quasi-normality [35] and adopt the ($\mathbf{k} \rightarrow 0$) aero-acoustic approximation, which is accurate for low Mach numbers and slightly overestimates the gravitational wave amplitude for Mach numbers approaching unity (for details see Sec. III of Ref. [18]). The final result is [18]

$$H_{ijij}(\mathbf{k}, \omega) \simeq H_{ijij}(0, \omega) = \frac{7C_K^2 \varepsilon}{6\pi^{3/2}} \int_{k_0}^{k_a} \frac{dk}{k^6} \exp\left(-\frac{\omega^2}{\varepsilon^{2/3} k^{4/3}}\right) \text{erfc}\left(-\frac{\omega}{\varepsilon^{1/3} k^{2/3}}\right). \quad (43)$$

Here, $\text{erfc}(x)$ is the complementary error function defined as $\text{erfc}(x) = 1 - \text{erf}(x)$, where $\text{erf}(x) = \int_0^x dy \exp(-y^2)$ is the error function [47]. The integral in Eq. (43) is dominated by the large scale ($k \simeq k_0$) contribution so, for direct-cascade turbulence during the first stage, the peak frequency is [18]

$$\omega_{\text{max}}^{(I)} \simeq k_0 M. \quad (44)$$

To compute the gravitational wave source during the second stage we consider Model A and Model B separately.

1. Model A

During the second stage, according to Eq. (30), kinetic energy can be neglected compared to magnetic energy. Proceeding as in the case of Kolmogorov turbulence and making use of the aero-acoustic approximation, we find

$$H_{ijij}(\mathbf{k}, \omega) \simeq H_{ijij}(0, \omega) = \frac{7C_1^2 M^3 \zeta_\star^{3/2}}{12\pi^{3/2} k_0} \int_{k_S}^{k_0} \frac{dk}{k^4} \exp\left(-\frac{\omega^2 k_0^2}{\zeta_\star M^2 k^4}\right) \text{erfc}\left(-\frac{\omega k_0}{\zeta_\star^{1/2} M k^2}\right), \quad (45)$$

where k_S can be found by saturating Eq. (35). In this case the integral is dominated by the large scale ($k \simeq k_S$) contribution and is maximal at

$$\omega_{\max}^{(II)} \simeq \frac{\zeta_*^{1/2} M k_S^2}{k_0} = 2\pi H_* . \quad (46)$$

2. Model B

In Model B of freely decaying MHD turbulence, as discussed in Sec. II.B.2, during the second stage kinetic energy is approximatively in equipartition with magnetic energy. To compute $H_{ijij}(\mathbf{k}, \omega)$, we proceed as for the case just discussed for Model A. The only differences reside in the expressions for the autocorrelation function and the smallest wavenumber where the inverse cascade stops, k_S [whose value can be found by saturating Eq. (41)]. For the case at hand we find

$$H_{ijij}(\mathbf{k}, \omega) \simeq H_{ijij}(0, \omega) = \frac{7C_1^2 M^3 \zeta_*^{3/2}}{6\pi^{3/2} k_0^{3/2}} \int_{k_S}^{k_0} \frac{dk}{k^{7/2}} \exp\left(-\frac{\omega^2 k_0}{\zeta_* M^2 k^3}\right) \text{erfc}\left(-\frac{\omega k_0^{1/2}}{\zeta_*^{1/2} M k^{3/2}}\right). \quad (47)$$

Again, the integral is dominated by the large scale ($k \simeq k_S$) contribution and is maximal at

$$\omega_{\max}^{(II)} \simeq \frac{\zeta_*^{1/2} M k_S^{3/2}}{k_0^{1/2}} = 2\pi H_* . \quad (48)$$

The fact that the frequency at the peak of the generated gravitational wave spectrum is independent of the particular model of turbulence [compare Eqs. (46) and (48)] is easily understood if one observes that it is the inverse of the maximum cascade timescale τ_{cas}^{\max} , which is $\tau_{\text{cas}}^{\max} = H_*^{-1}$ by definition.

IV. GRAVITATIONAL WAVE SPECTRA

The total gravitational wave energy density spectrum $\rho_{\text{GW}}(\omega)$ at a given space-time event is obtained by integrating over all source regions with a light-like separation from that event, and includes contributions from gravitational wave generated during the first and second stages. For the first stage (with duration time $\tau_T^{(I)} = s_0 \tau_0$) $\rho_{\text{GW}}^{(I)}(\omega)$ is given by Eqs. (21) and (A3) of Ref. [18]. For the second stage contribution we must account for the scale dependence of the cascade time. The total GW fractional energy density parameter at the moment of emission is [18]

$$\Omega_{\text{GW}}(\omega_*) \simeq 105 \frac{H_*^4 \omega^3}{H_0^2} \sum_m \tau_T^{(m)} H_{ijij}^{(m)}(0, \omega_*). \quad (49)$$

Here the index m runs over I and II for the first and second decay stages, $\omega_* = \omega(t_*)$ is the angular frequency of the gravitational wave at the moment of its emission, and H_0 is the current value of the Hubble parameter.

The current gravitational wave amplitude is related to the current fractional energy density parameter through

$$h_C(f) = 1.26 \times 10^{-18} \left(\frac{\text{Hz}}{f}\right) [h_0^2 \Omega_{\text{GW}}(f)]^{1/2}, \quad (50)$$

where h_0 is the current Hubble parameter in units of $100 \text{ km sec}^{-1} \text{ Mpc}^{-1}$ [3]. Using the expressions found for the H_{ijij} tensor, we obtain

$$h_C(f) \simeq 2 \times 10^{-14} \left(\frac{100 \text{ GeV}}{T_*}\right) \left(\frac{100}{g_*}\right)^{1/3} \sum_m \left[\tau_T^{(m)} \omega_* H_*^4 H_{ijij}^{(m)}(0, \omega_*)\right]^{1/2}. \quad (51)$$

Here, $f = (a_*/a_0)f_*$ is the linear frequency, with $f_* = \omega_*/2\pi$.

Figure 1 shows the gravitational wave amplitudes, $h_C(f)$, from pure hydrodynamical turbulence (no inverse cascade) and for Models A and B for two different values of initial magnetic helicity, $\zeta_* = 0.15$ (left panel) and $\zeta_* = 0.05$ (right panel). Accounting for inverse-cascade MHD turbulence, the gravitational wave spectrum has two peaks: the first higher-frequency one is associated with direct-cascade hydrodynamical turbulence while the second lower-frequency

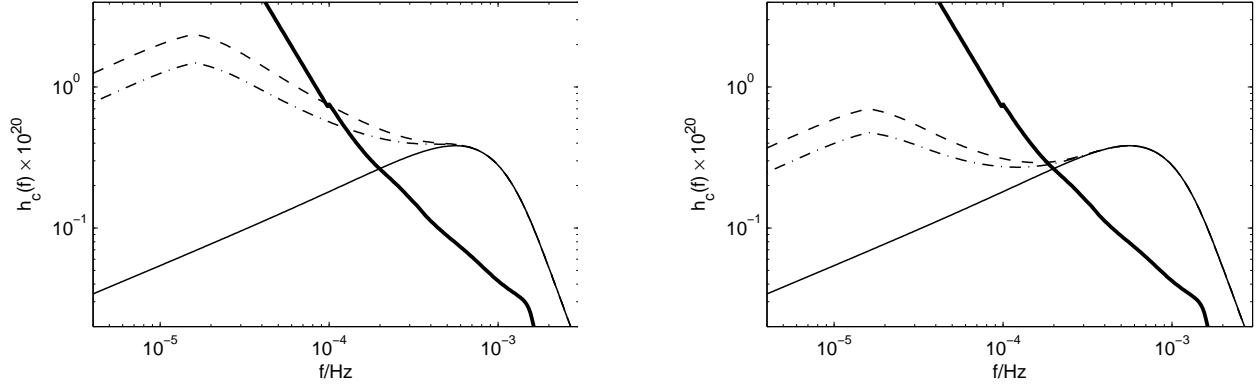


FIG. 1: The spectrum of the gravitational wave strain amplitude, $h_C(f)$, as a function of the frequency f for a first-order phase transition with $g_* = 100$, $T_* = 100$ GeV, $\alpha = 0.5$, and $\beta = 100H_*$, from hydrodynamic Kolmogorov turbulence with zero magnetic helicity (solid lines) and for the two MHD turbulence models, Model A (dash-dotted lines) and Model B (dashed lines). The left panel corresponds to initial magnetic helicity $\zeta_* = 0.15$, while $\zeta_* = 0.05$ in the right panel. In both panels the bold solid line corresponds to the 1-year, 5σ LISA design sensitivity curve [48] including confusion noise from white dwarf binaries [49].

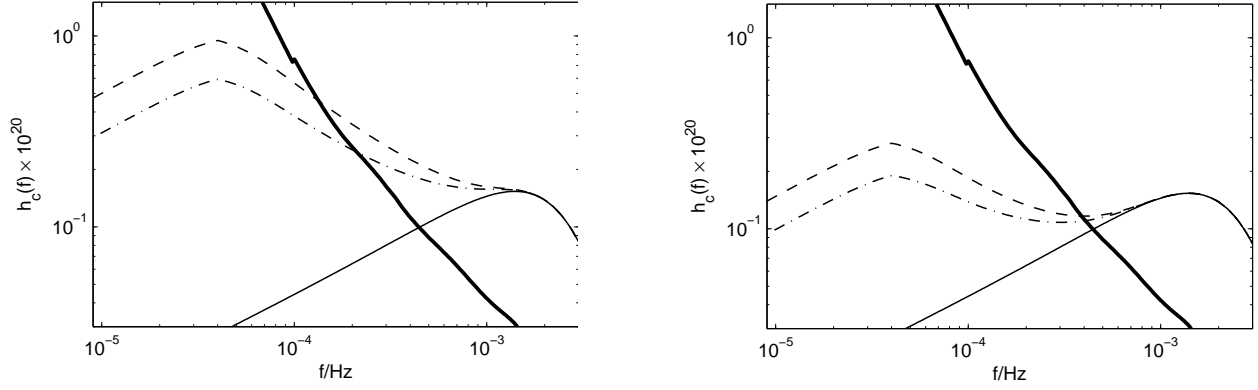


FIG. 2: As in Fig. 1, except now $T_* = 250$ GeV.

one is induced by inverse-cascade MHD turbulence. The amplitude of gravitational waves emitted during direct-cascade unmagnetized turbulence peaks at current frequency [10, 15, 16, 18, 28]

$$f_{\max}^{(I)} = \frac{Mk_0}{2\pi} \frac{a_*}{a_0} = \left(\frac{M}{v_b}\right) \left(\frac{\beta}{H_*}\right) f_H. \quad (52)$$

Here we have used $2\pi/k_0 = l_0 = v_b\beta^{-1}$, where v_b is the bubble wall velocity, and defined

$$f_H = H_* \frac{a_*}{a_0} \simeq 1.6 \times 10^{-5} \text{ Hz} \left(\frac{g_*}{100}\right)^{1/6} \left(\frac{T_*}{100 \text{ GeV}}\right). \quad (53)$$

The second peak is at a lower frequency compared to the unmagnetized case and is independent of the adopted turbulence model (since it is determined by the Hubble frequency at the moment of gravitational wave generation). In fact, the second peak frequency is

$$f_{\max}^{(II)} = f_H. \quad (54)$$

Finally, as it is straightforward to establish, the amplitude of MHD-turbulence-generated gravitational waves at the peak in Model A is about a factor $(M/\gamma)^{3/4}\zeta_*^{9/8}$ larger than that in the unmagnetized case (and thus strongly depends on initial magnetic helicity), while it is about a factor $\sqrt{2}(M/\gamma)^{1/12}\zeta_*^{1/24}$ smaller than that in Model B.

In Fig. 2 we show the strain amplitude $h_C(f)$ for a higher phase transition temperature, $T_* = 250$ GeV, with the rest of the parameters taking the same values as in Fig. 1. Comparing Figs. 1 and 2 we see that if the phase transition occurs at higher energy the peak frequency is higher, closer to the LISA design sensitivity peak.

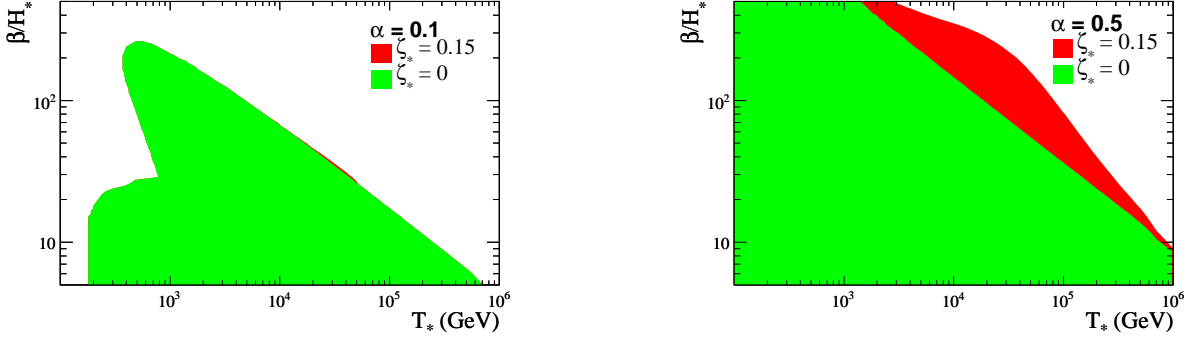


FIG. 3: The LISA sensitivity region for Model A in the β/H_* and T_* parameter plane for a phase transition with vacuum energy $\alpha = 0.1$ (left panel) and $\alpha = 0.5$ (right panel) [28]. The regions for $\zeta_* = 0$ and $\zeta_* = 0.15$ coincide at these temperatures for $\alpha = 0.1$ (left panel). A point in parameter space is considered detectable if at any frequency its value of $h_c(f)$ is detectable at a signal-to-noise ratio of 5 in a one-year integration, including the confusion noise from white dwarf binaries, based on Refs. [48].

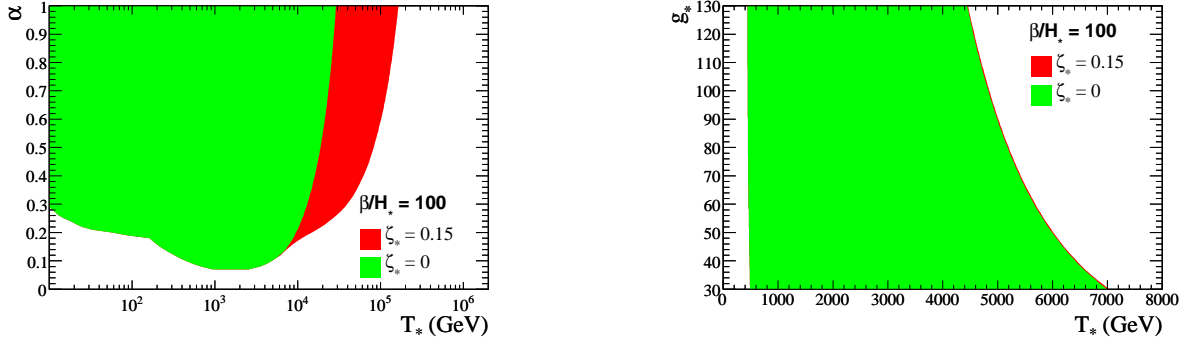


FIG. 4: The LISA sensitivity region for Model A in the α and T_* parameter plane (left panel) with $\beta/H_* = 100$ and $g_* = 100$, and in the g_* and T_* parameter plane (right panel) with $\beta/H_* = 100$ and $\alpha = 0.1$. A point in parameter space is considered detectable if at any frequency its value of $h_c(f)$ is detectable at a signal-to-noise ratio of 5 in a one-year integration, including the confusion noise from white dwarf binaries, based on Refs. [48].

The gravitational wave signal detection prospects depends crucially on several parameters: the temperature (the energy scale) at which the phase transition takes place T_* , the number of relativistic degree of freedom g_* , the phase transition model parameters α and β/H_* , and the initial magnetic helicity.

The dependence on g_* is quite weak, see Eq. (51). It affects both peak frequencies (associated with hydrodynamical and MHD turbulence). The initial magnetic helicity plays a more substantial role if the phase transition takes places at a higher temperature [28]. The phase transition model determines the value of the parameter α . The tensor H_{ijij} appearing in Eq. (51) depends on α as well as on the duration time of the direct cascade stage $\tau_T^{(I)}$ [18]. In addition, the frequency of the first peak ($\sim k_0 M$) depends on α through the bubble wall velocity (v_b) and other parameters, see Eqs. (13)–(15). Increasing α makes the gravitational wave signal stronger, see Fig. 2 of Ref. [28]. In the context of the detection of gravitational waves, the phase transition energy scale has two different effects: the peak frequency is proportional to T_* but the peak amplitude is inversely proportional to T_* . These effects must be accounted for together, see Fig. 3 of Ref. [28]. Another important parameter is β/H_* which is model dependent and affects the first peak frequency, see Eq. (52), as well as the amplitude of the gravitational wave signal. The dependence on β/H_* can be seen in Fig. 5 of Ref. [28]: a larger β/H_* results in a lower amplitude signal with a higher first-peak frequency, while the position of the second peak, associated with inverse-cascade turbulence, is not affected. Figure 3 shows the LISA sensitivity region in the β/H_* and T_* parameter plane for a phase transition with vacuum energy $\alpha = 0.1$ (left panel) and $\alpha = 0.5$ (right panel) for Model A. Figure 4 shows the LISA sensitivity regions in the α and T_* parameter plane (left panel) and in the g_* and T_* parameter plane (right panel) for Model A.

V. CONCLUSION

We have analyzed the generation of gravitational waves at the electroweak phase transition, from hydrodynamic turbulence in the presence of a helical magnetic field. It is convenient to consider this as a two-stage process. During the first stage the effects of helicity are negligible when studying the production of gravitational waves from turbulence. The first stage ends when quasi-conservation of magnetic helicity starts to trigger an inverse cascade of the magnetic field, that is, a transfer of magnetic energy from small to large scales. The details of the inverse cascade process in helical MHD are still under debate and there exist in the literature two different models. In this paper we have examined gravitational wave generation in both models of helical MHD turbulence. We have found that, for realistic values of the parameters defining the electroweak phase transition, the generated gravitational wave spectrum is independent of turbulence modeling (within a factor of order 2).

The inverse-cascade associated peak frequency always coincides with the Hubble frequency at the moment of gravitational wave production. Moreover, as clear from Fig. 1, the main contribution to the total gravitational waves energy density is from the second, inverse-cascade stage, even for small values of magnetic helicity.

Gravitational waves produced *via* helical turbulence are strongly polarized, since magnetic helicity is a parity-odd quantity and is maximal at the end of the first stage [17]. LISA should be able to detect such a gravitational wave polarization [22]. Also, in contrast to the unmagnetized case, the contribution to the gravitational wave amplitude coming from the inverse-cascade stage is large enough at 0.1 mHz to be detectable by LISA. If the electroweak phase transition occurs at higher energy (see Fig. 2) the peak frequency is higher, closer to the LISA sensitivity peak, which leads to a stronger signal. Our formalism is also applicable to gravitational wave production at an earlier QCD phase transition, assuming the presence of colored magnetic fields [50], or to any other phase transition [6]: the peak frequency will shift according to changes in T_* and g_* .

Finally, we stress that the gravitational wave signal arising from helical MHD turbulent motion exceeds that from bubble collisions [7, 24, 25] and that from hydrodynamical turbulence alone [10, 18]. Of course, the strong signal estimated here (see also Ref. [1]) assumes initial non-zero (although small) magnetic helicity, so detection of polarized gravitational waves by LISA will indicate parity violation during the phase transition, as proposed in Refs. [20].

Acknowledgments

We acknowledge helpful discussions with R. Durrer, A. Gruzinov, A. Kosowsky, and G. Lavrelashvili. G.G. and T.K. acknowledge the hospitality of the Abdus Salam International Center for Theoretical Physics, and support from INTAS grant 061000017-9258 and Georgian NSF grants ST06/4-096 and ST07/4-193. T.K., Y.M., and B.R. acknowledge US DOE grant DE-FG03-99EP41093.

-
- [1] T. Kahniashvili, G. Gogoberidze, and B. Ratra, Phys. Rev. Lett. **100**, 231301 (2008).
 - [2] S. Chongchitnan and G. Efstathiou, Phys. Rev. D **73**, 083511 (2006); C. J. Hogan, AIP Conf. Proc. **873**, 30 (2006); A. Buonanno, arXiv:0709.4682 [qr-qc].
 - [3] M. Maggiore, Phys. Rept. **331**, 28 (2000).
 - [4] L. P. Grishchuk, Sov. Phys. JETP **40**, 409 (1975) [Zh. Eksp. Teor. Fiz. **67**, 825 (1974)]; A. Starobinsky, Sov. Phys. JETP Lett. **30**, 682 (1979) [Pisma Zh. Eksp. Teor. Fiz. **30**, 719 (1979)]; V. A. Rubakov, M. V. Sazhin, and A. V. Veryaskin, Phys. Lett. B **115**, 189 (1982); B. Allen, Phys. Rev. D **37**, 2078 (1988); B. Ratra, Phys. Rev. D **45**, 1913 (1992); M. Giovannini, Phys. Rev. D **60**, 123511 (1999).
 - [5] J. F. Dufaux, *et al.*, Phys. Rev. D **76**, 123517 (2007); R. Easther, J. T. Giblin, and E. A. Lim, Phys. Rev. D **77**, 103519 (2008); J. Garcia-Bellido, D. G. Figueroa, and A. Sastre, Phys. Rev. D **77**, 043517 (2008).
 - [6] E. Witten, Phys. Rev. D **30**, 272 (1984); C. J. Hogan, Mon. Not. R. Astron. Soc. **218**, 629 (1986); M. S. Turner and F. Wilczek, Phys. Rev. Lett. **65**, 3080 (1990); A. Kosowsky, M. S. Turner, and R. Watkins, Phys. Rev. D **45**, 4514 (1992).
 - [7] M. Kamionkowski, A. Kosowsky, and M. S. Turner, Phys. Rev. D **49**, 2837 (1994); R. A. A. Abreu, *et al.*, Class. Quant. Grav. **18**, L155 (2001); A. Megevand, arXiv:0804.0391 [astro-ph].
 - [8] S. J. Huber and T. Konstandin, JCAP **0805**, 017 (2008); arXiv:0806.1828 [hep-ph].
 - [9] C. Caprini, R. Durrer, and G. Servant, Phys. Rev. D **77**, 124015 (2008).
 - [10] A. Nicolis, Class. Quant. Grav. **21**, L27 (2004).
 - [11] T. Vachaspati and A. Vilenkin, Phys. Rev. D **31**, 3052 (1985); M. P. Infante and N. Sánchez, Phys. Rev. D **61**, 083515 (2000).
 - [12] D. V. Deriagin, *et al.*, Mon. Not. R. Astron. Soc. **229**, 357 (1987); R. Durrer, P. Ferreira, and T. Kahniashvili, Phys. Rev. D **61**, 043001 (2000); A. Lewis, Phys. Rev. D **70**, 043011 (2004).
 - [13] C. Caprini, R. Durrer, and T. Kahniashvili, Phys. Rev. D **69**, 063006 (2004).

- [14] C. Caprini and R. Durrer, Phys. Rev. D **74**, 063521 (2006).
- [15] A. Kosowsky, A. Mack, and T. Kahniashvili, Phys. Rev. D **66**, 024030 (2002).
- [16] A. D. Dolgov, D. Grasso, and A. Nicolis, Phys. Rev. D **66**, 103505 (2002).
- [17] T. Kahniashvili, G. Gogoberidze, and B. Ratra, Phys. Rev. Lett. **95**, 151301 (2005).
- [18] G. Gogoberidze, T. Kahniashvili, and A. Kosowsky, Phys. Rev. D **76**, 083002 (2007).
- [19] <http://lisa.nasa.gov/>
- [20] For primordial magnetic helicity production models, see, e.g., J. Cornwall, Phys. Rev. D **56**, 6146 (1997); M. Giovannini and M. E. Shaposhnikov, Phys. Rev. D **57**, 2186 (1998); G. B. Field and S. M. Carroll, Phys. Rev. D **62**, 103008 (2000); T. Vachaspati, Phys. Rev. Lett. **87**, 251302 (2001); G. Sigl, Phys. Rev. D **66**, 123002 (2002); K. Subramanian and A. Brandenburg, Phys. Rev. Lett. **93**, 205001 (2004); L. Campanelli and M. Giannotti, Phys. Rev. D **72**, 123001 (2005); V. B. Semikoz and D. D. Sokoloff, Astron. Astrophys. **413**, L53 (2005); A. Diaz-Gil, J. Garcia-Bellido, M. Garcia Perez and A. Gonzalez-Arroyo, Phys. Rev. Lett. **100**, 241301 (2008); L. Campanelli, arXiv:0805.0575 [astro-ph]; L. Campanelli, P. Cea, and G. L. Fogli, arXiv:0805.1851 [astro-ph].
- [21] A. Lue, L. M. Wang, and M. Kamionkowski, Phys. Rev. Lett. **83**, 1506 (1999); D. Lyth, C. Quimbay, and Y. Rodriguez, JHEP **0503**, 016 (2005); M. Satoh, S. Kanno, and J. Soda, Phys. Rev. D **77**, 023526 (2008).
- [22] N. Seto, Phys. Rev. Lett. **97**, 151101 (2006).
- [23] S. H. S. Alexander, M. E. Peskin, and M. M. Sheikh-Jabbari, Phys. Rev. Lett. **96**, 081301 (2006); S. Saito, K. Ichiki, and A. Taruya, JCAP **0709**, 002 (2007).
- [24] R. Aureda, *et al.*, Nucl. Phys. B **631**, 342 (2002); A. Nicolis, Class. Quant. Grav. **21**, L27 (2004).
- [25] C. Grojean and G. Servant, Phys. Rev. D **75**, 043507 (2007).
- [26] C. Delaunay, C. Grojean, and J. D. Wells, JHEP **0804**, 029 (2008).
- [27] M. Pietroni, Nucl. Phys. B **402**, 27 (1993); A. T. Davies, C. D. Froggatt, and R. G. Moorhouse, Phys. Lett. B **372**, 88 (1996); S. J. Huber and M. G. Schmidt, Eur. Phys. J. C **10**, 473 (1999); C. Balazs, M. S. Carena, A. Freitas, and C. E. M. Wagner, JHEP **0706**, 066 (2007).
- [28] T. Kahniashvili, A. Kosowsky, G. Gogoberidze, and Y. Maravin, Phys. Rev. D **78**, 043003 (2008).
- [29] L. Randall and G. Servant, JHEP **0705**, 054 (2007).
- [30] D. Biskamp and W.-C. Müller, Phys. Rev. Lett. **83**, 2195 (1999); Phys. Plasma **7**, 4889 (2000).
- [31] M. Christensson, M. Hindmarsh, and A. Brandenburg, Phys. Rev. E **64**, 056405 (2001); Astron. Nachrichten **326**, 393 (2005).
- [32] D. T. Son, Phys. Rev. D **59**, 063008 (1999).
- [33] R. Banerjee and K. Jedamzik, Phys. Rev. Lett. **91**, 251301 (2003) [Erratum-ibid. **93**, 179901 (2004)]; Phys. Rev. D **70**, 123003 (2004).
- [34] L. Campanelli, Phys. Rev. Lett. **98**, 251302 (2007).
- [35] A. S. Monin and A. M. Yaglom, *Statistical Fluid Mechanics* (MIT Press, Cambridge, MA, 1975).
- [36] M. E. Goldstein, *Aeroacoustics* (McGraw-Hill, New York, 1976).
- [37] M. J. Lighthill, Proc. R. Soc. London A **211**, 564 (1952); **222**, 1 (1954).
- [38] I. Proudman, Proc. R. Soc. London A **214**, 119 (1952).
- [39] M. S. Turner, R. Watkins, and L. M. Widrow, Astrophys. J. Lett. **367**, L43 (1991).
- [40] S. Weinberg, *Gravitation and Cosmology* (Wiley & Sons, New York, 1972).
- [41] e.g., B. Ratra and M. S. Vogeley, Publ. Astron. Soc. Pac. **120**, 235 (2008).
- [42] P. J. Steinhardt, Phys. Rev. D **25**, 2082 (1982).
- [43] J. V. Shebalin, W. H. Matthaeus, and D. Montgomery, J. Plasma Phys. **29**, 525 (1983); P. Goldreich and S. Sridhar, Astrophys. J. **438**, 763 (1995).
- [44] R. H. Kraichnan, Phys. Fluids **7**, 1163 (1964).
- [45] D. Biskamp, *Magnetohydrodynamic Turbulence* (Cambridge University, Cambridge, 2003); M. K. Verma, Phys. Rept. **401**, 229 (2004).
- [46] A. N. Kolmogorov, Dokl. Akad. Nauk. SSSR **30**, 299 (1941) [Proc. R. Soc. London A **434**, 9 (1991)].
- [47] I. S. Gradshteyn and I. M. Ryzhik, *Table of Integrals, Series, and Products, Sixth Edition* (Academic Press, San Diego, CA, 2000).
- [48] S. L. Larsen, W. A. Hiscock, and R. W. Hellings, Phys. Rev. D **62**, 062001 (2000); N. Cornish, Phys. Rev. D **65**, 022004 (2001). For the LISA sensitivity curve calculator used here see <http://www.srl.caltech.edu/~shane/sensitivity/>.
- [49] P. L. Bender and D. Hils, Class. Quant. Grav. **14**, 1439 (1997).
- [50] M. H. P. van Putten, Phys. Rev. D **50**, 6640 (1994).